Scilight

Intelligence & Control
https://www.sciltp.com/journals/ic



Article

Check for updates

Further on Time-Varying Formation Control for Directed Networks with Switching Topologies

Beibei Zhang [1], Hong Sang [1,*], Yi Liu [1], Peng Wang [2] and Georgi M. Dimirovski [3]

[1] College of Marine Electrical Engineering, Dalian Maritime University, Dalian 116026, China
[2] School of Mathematics and Statistics, Fuzhou University, Fuzhou 350108, China
[3] Doctoral School FEIT, SS Cyril and Methodius University, 1000 Skopje, North Macedonia
* Correspondence: sanghong@dlmu.edu.cn

How To Cite: Zhang, B.; Sang, H.; Liu, Y.; et al. Further on Time-Varying Formation Control for Directed Networks with Switching Topologies. *Intelligence & Control* **2026**, *2*(4), 2. https://doi.org/10.53941/ic.2026.100016

Received: 23 July 2026
Revised: 9 September 2026
Accepted: 6 October 2026
Published: 30 October 2026

Abstract: In this research, the time-varying formation (TVF) control problem is examined for general directed networks (DNs) subject to switching communication topologies, which widely arises in cooperative tasks of multiple mobile robots. In such practical scenarios, time-varying communication links induced by obstacles, agent mobility and bandwidth limitations bring nontrivial challenges for reliable formation maintenance. To address this issue, a distributed formation control protocol is developed by utilizing local formation error feedback, topology-dependent relative formation error coupling, a positive coupling strength, and a formation compensation signal. By virtue of the constructed control protocol combined with a nonsingular coordinate transformation, the anticipated TVF control task is recast as an exponential stability verification issue of a general switched system. Then, upon constructing an innovative topology-dependent time-varying Lyapunov function (TDTVLF) approach together with the dwell-time switching (DTS) strategy, the corresponding sufficient conditions are then derived to guarantee the exponential convergence of the formation error dynamics. Finally, the formation control of multiple mobile robots is carried out to validate the effectiveness and practical applicability of the proposed TVF control protocol.

Keywords: time-varying formation control; directed networks; topology-dependent time-varying Lyapunov function; switching topologies

1. Introduction

DNs represent a class of complex dynamical systems consisting of multiple coupled nodes interacting under designated communication topologies. Such inherent characteristics enable numerous practical complex systems to be efficiently described within the directed network framework [1–5]. Accordingly, cooperative control of DNs has garnered substantial research interest in recent years, due to its extensive application prospects in unmanned aerial vehicles, mobile robots, autonomous underwater vehicles, satellite formations, and intelligent transportation systems. Among various cooperative control problems, formation control constitutes a pivotal research direction, whose objective is to drive a group of network nodes to achieve and maintain a prescribed geometric pattern by using local information exchange [6]. In prior literature, the adopted formation control methods mainly include the leader-follower approach, the behavior-based approach, and the virtual-structure-based approach [7–9]. As the field advanced, consensus and graph-theoretic techniques established a universal distributed analytical framework to unify formation control analysis over DNs [10–13].

In practical tasks such as cooperative surveillance, target encirclement, obstacle avoidance, and environmental monitoring, network nodes are often required to adjust their relative positions according to time-varying mission requirements. Therefore, TVF control stands out as an indispensable research direction in the field of DNs. A wealth of existing literature has investigated formation control issues for first-order, second-order, high-order, and general linear multi-agents under different communication topologies [14–17]. Nevertheless, the majority of these

Copyright: © 2026 by the authors. This is an open access article under the terms and conditions of the Creative Commons Attribution (CC BY) license (https://creativecommons.org/licenses/by/4.0/).
Publisher's Note: Scilight stays neutral with regard to jurisdictional claims in published maps and institutional affiliations.

established achievements are confined to static formation configurations, oversimplified node dynamics, or fixed/undirected interaction topologies. Practical communication networks generally exhibit directed features and may undergo frequent topology switching caused by restricted sensing coverage, data packet dropout, communication bandwidth limitations and external environmental perturbations. To date, extensive investigations have been conducted on formation control for DNs subject to switching communication topologies [16–20]. A variety of results with both theoretical novelty and practical engineering significance have been derived via switched system theory. For example, utilizing dwell-time switching constraints together with multiple Lyapunov function theory, the study [16] derived necessary and sufficient solvability conditions for TVF of linear multi-agent systems under switching directed topologies. It was proven that the desired formation can be achieved provided that the prescribed TVF belongs to the feasible formation set and that the dwell time for topology switching exceeds some positive threshold. By adopting the common Lyapunov function method, the work [17] developed an adaptive output-feedback distributed TVF control scheme that utilizes local output information for linear swarm systems under both fixed and switching topologies. Corresponding control protocols and adaptive mechanisms were devised for these two topology categories to attain the prescribed formation performance. For nonlinear multi-agent systems with directed switching topologies, the fault-tolerant formation control problem was investigated in [18], where a distributed fuzzy formation controller was synthesized to guarantee the uniform ultimate boundedness of formation errors.

Furthermore, the reference formation vector together with its time derivative jointly exerts a coupling influence on the closed-loop dynamics within the TVF control framework. Accordingly, arbitrary predefined time-varying formations are not always attainable for the examined DNs. Under such circumstances, it becomes imperative to characterize the collection of feasible time-varying formations and construct a distributed control protocol capable of ensuring formation error convergence under switching directed communication topologies. Trajectory tracking generally requires agents to follow prescribed reference trajectories, whereas formation control specifies the desired relative geometric relationships among agents. The overall macroscopic motion of the entire formation emerges autonomously from the closed-loop evolution rather than being pre-specified. Therefore, it is necessary to determine which prescribed time-varying formations are achievable and how the corresponding formation reference function is produced. The feasibility condition derived in [16] shows that the desired formation must satisfy a constraint determined by the agent dynamics, the input matrix, and the switching directed topology. Nevertheless, developing stabilizing protocols with reduced conservatism for the derived reduced-order switched error dynamics still remains challenging.

Motivated by the above observations, this paper studies the TVF control problem for general DNs under switching topologies. A distributed formation control protocol equipped with topology-dependent coupling gains and a nonsingular coordinate transformation are jointly adopted to convert the original time-varying formation (TVF) control problem into a stability analysis framework for the reduced-order switched error system. A compensation signal is further designed to extend the feasible set of time-varying formations. Different from the Lyapunov function approach as in [16] for the formation control over DNs with switching topologies, this paper develops a novel formation control framework via the construction of a TDTVLF technique combined with the DTS mechanism, and further derives the corresponding sufficient criteria to ensure exponential convergence of the formation error. To conclude, the validity and practicability of the developed methodology are verified via numerical simulations of multi-robot formation control scenarios.

Notation: In this research, $\mathbb{R}^n$ and $\mathbb{R}^{m\times n}$ denote the n-dimensional Euclidean space and the set of all $m\times n$ real matrices, respectively; $\mathbf{I}_m$ and $\mathbf{0}_{m\times n}$ represent the $m\times m$ identity matrix and the $m\times n$ zero matrix, respectively; $\mathbf{1_N}$ signifies the $\mathbf{N}$-dimensional column vector $[1,1,\ldots,1]^{\mathrm{T}}$; $\boldsymbol{\lambda}_{\min}(\mathbf{A})$, $\boldsymbol{\lambda}_{\max}(\mathbf{A})$ and $\boldsymbol{\lambda}_i(\mathbf{A})$ refer to the minimum, maximum and the i-th eigenvalue of the square matrix $\mathbf{A}$; $\mathbb{N}$ and $\mathbb{N}_+$ correspond to the set of natural numbers and positive integers; $\mathbb{S}_{[a,b]}$ with $a\le b\in\mathbb{N}$ defines the set $[a,b]\cap\mathbb{N}$; $\otimes$ represents the Kronecker product; $\mathbf{Sym}(\mathbf{A})$ is defined as $\mathbf{A}+\mathbf{A}^{\mathrm{T}}$; $\mathbf{col}(\cdot)$ and $\mathbf{diag}(\cdot)$ represent the block-column vector and block-diagonal matrix, while $\mathbf{col}(\omega_i)_{i=1}^{\mathbf{N}}$ is short for $\mathbf{col}(\omega_1,\omega_2,\ldots,\omega_{\mathbf{N}})$ and $\mathbf{diag}(\omega_i)_{i=1}^{\mathbf{N}}$ is short for $\mathbf{diag}(\omega_1,\omega_2,\ldots,\omega_{\mathbf{N}})$; finally, $\mathbf{Re}\big(\boldsymbol{\lambda}_i(\mathbf{A})\big)$ corresponds to the real part of $\boldsymbol{\lambda}_i(\mathbf{A})$.

2. Preliminaries and Problem Formulation

Consider a DN consisting of $\mathbf{N}$ nodes with the dynamics of the i-th node described by

$$\dot{\boldsymbol{x}}_i(t)=\mathbf{A}\boldsymbol{x}_i(t)+\mathbf{B}\boldsymbol{u}_i(t),\quad i\in\mathbb{S}_{[1,\mathbf{N}]},\tag{1}$$

where $\boldsymbol{x}_i(t)=[\boldsymbol{x}_{i1}^{\mathrm{T}}(t),\boldsymbol{x}_{i2}^{\mathrm{T}}(t),\cdots,\boldsymbol{x}_{i\mathbf{p}}^{\mathrm{T}}(t)]^{\mathrm{T}}\in\mathbb{R}^{\mathbf{p}}$ and $\boldsymbol{u}_i(t)=[\boldsymbol{u}_{i1}^{\mathrm{T}}(t),\boldsymbol{u}_{i2}^{\mathrm{T}}(t),\cdots,\boldsymbol{u}_{i\mathbf{q}}^{\mathrm{T}}(t)]^{\mathrm{T}}\in\mathbb{R}^{\mathbf{q}}$ denote the state and control input of the i-th node, respectively. The matrices $\mathbf{A}$ and $\mathbf{B}$ are constant system matrices with appropriate dimensions, where $\mathbf{B}$ possesses full column rank, i.e., $\mathbf{rank}(\mathbf{B})=\mathbf{q}$.

The anticipate TVF is described by $\boldsymbol{y}(t)=\mathbf{col}\big(\boldsymbol{y}_i(t)\big)_{i=1}^{\mathbf{N}}\in\mathbb{R}^{\mathbf{Np}}$, in which $\boldsymbol{y}_i(t)\in\mathbb{R}^{\mathbf{p}}$ for all indices

$i \in \mathbb{S}_{[1,\mathbf{N}]}$. Besides, every $\boldsymbol{y}_i(t)$ is piecewise continuously differentiable, characterizing the expected relative displacement of node i inside the predefined formation geometry. Accordingly, the investigated TVF is formalized in the following definition.

Definition 1 ([16]). *The DN (1) is regarded to realize the TVF prescribed by $\boldsymbol{y}(t)$, if there exists a vector-valued function $\boldsymbol{\hbar}(t) \in \mathbb{R}^{\mathbf{p}}$ such that*

$$\lim_{t\to\infty} \big(\boldsymbol{x}_i(t) - \boldsymbol{y}_i(t) - \boldsymbol{\hbar}(t)\big) = 0, \quad i \in \mathbb{S}_{[1,\mathbf{N}]}, \tag{2}$$

in which $\boldsymbol{\hbar}(t)$ is called the formation reference function.

For the DN (1) incorporating $\mathbf{N}$ individual nodes, the switching interaction topologies among nodes are formulated by directed graphs $\mathcal{G}_{\varsigma(t)} = (\boldsymbol{\upsilon}, \mathbf{E}_{\varsigma(t)}, \mathbf{W}_{\varsigma(t)})$, where $\boldsymbol{\upsilon} = \mathbb{S}_{[1,\mathbf{N}]}$ stands for the collection of network nodes, $\mathbf{E}_{\varsigma(t)} \subseteq \boldsymbol{\upsilon} \times \boldsymbol{\upsilon}$ characterizes all directed connection pairs, and $\mathbf{W}_{\varsigma(t)} = [\boldsymbol{w}_{ij}^{\varsigma(t)}]_{\mathbf{N}\times\mathbf{N}} \in \mathbb{R}^{\mathbf{N}\times\mathbf{N}}$ corresponds to the weighted adjacency matrix. $\varsigma(t) : [0, +\infty) \to \aleph := \mathbb{S}_{[1,\varsigma_{\text{num}}]}$ determines the switching signal, representing the active interaction topology at time t. For any $i \neq j$, the existence of directed link $(j, i) \in \mathbf{E}_{\varsigma(t)}$ implies that node i is capable of acquiring information originating from node j. Meanwhile, the corresponding adjacency weight satisfies $\boldsymbol{w}_{ij}^{\varsigma(t)} = 1$, whereas $\boldsymbol{w}_{ij}^{\varsigma(t)} = 0$ otherwise. Additionally, it is stipulated that $\boldsymbol{w}_{ii}^{\varsigma(t)} = 0$ for all $i \in \boldsymbol{\upsilon}$. The neighbor set of the node i within the directed graphs $\mathcal{G}_{\varsigma(t)}$ is defined as $\aleph_{\varsigma(t)}^{i} = \{j \in \boldsymbol{\upsilon} : (j, i) \in \mathbf{E}_{\varsigma(t)}\}$. The in-degree associated with the node i is calculated by $\mathbf{d}_{\varsigma(t)}^{i} = \sum_{j=1}^{\mathbf{N}} \boldsymbol{w}_{ij}^{\varsigma(t)}$. Consequently, the Laplacian matrix corresponding to the directed graphs $\mathcal{G}_{\varsigma(t)}$ can be expressed as $\mathcal{L}_{\varsigma(t)} = \mathbf{D}_{\varsigma(t)} - \mathbf{W}_{\varsigma(t)}$, where $\mathbf{D}_{\varsigma(t)} = \mathbf{diag}(\mathbf{d}_{\varsigma(t)}^{1}, \mathbf{d}_{\varsigma(t)}^{2}, \ldots, \mathbf{d}_{\varsigma(t)}^{\mathbf{N}})$.

Within this context, all network nodes are required to track the predefined relative geometric layout, whereas the overall formation moves according to the formation reference $\boldsymbol{\hbar}(t)$. Figure 1 presents the schematic diagram for the proposed TVF control framework. To achieve the target TVF under switching topologies, the following distributed formation control protocol is considered:

$$\boldsymbol{u}_i(t) = \mathbf{K}_1\big(\boldsymbol{x}_i(t) - \boldsymbol{y}_i(t)\big) + \boldsymbol{\alpha}\mathbf{K}_{2,\varsigma(t)} \sum_{j\in\aleph_{\varsigma(t)}^{i}} \boldsymbol{w}_{ij}^{\varsigma(t)} \Big[\big(\boldsymbol{x}_j(t) - \boldsymbol{y}_j(t)\big) - \big(\boldsymbol{x}_i(t) - \boldsymbol{y}_i(t)\big)\Big] + \boldsymbol{c}_i(t), \tag{3}$$

where $\mathbf{K}_1$ is a constant feedback gain, $\boldsymbol{\alpha} > 0$ is the coupling strength, and $\mathbf{K}_{2,\varsigma(t)}$ is a topology-dependent coupling gain. Moreover, $\boldsymbol{c}_i(t) \in \mathbb{R}^{\mathbf{q}}$ signifies the formation compensation signal associated with the desired TVF.

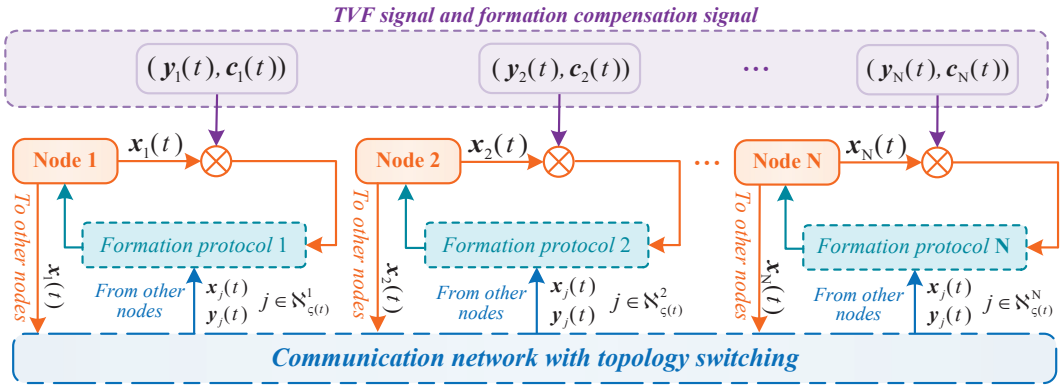


Figure 1. Schematic diagram for the proposed TVF control framework.

Remark 1. *In this research, each possible directed topology $\mathcal{G}_{\varsigma(t)}$ contains a spanning tree. Then, zero constitutes a simple eigenvalue of $\mathcal{L}_{\varsigma(t)}$, whose corresponding right eigenvector is the all-one vector $\mathbf{1}_{\mathbf{N}}$, while the remaining $\mathbf{N} - 1$ eigenvalues of $\mathcal{L}_{\varsigma(t)}$ possess positive real parts. Define the nonsingular matrix $\mathfrak{F} = \begin{bmatrix}\boldsymbol{\nu}_1 & \tilde{\mathfrak{F}}\end{bmatrix} \in \mathbb{R}^{\mathbf{N}\times\mathbf{N}}$, where $\boldsymbol{\nu}_1 = \mathbf{1}_{\mathbf{N}}$ and $\tilde{\mathfrak{F}} = [\boldsymbol{\nu}_2 \ \ \boldsymbol{\nu}_3 \ \ \cdots \ \ \boldsymbol{\nu}_{\mathbf{N}}] \in \mathbb{R}^{\mathbf{N}\times(\mathbf{N}-1)}$. Denote $\mathfrak{F}^{-1} = \begin{bmatrix}\bar{\boldsymbol{\nu}}_1^{\mathrm{T}} & \bar{\mathfrak{F}}^{\mathrm{T}}\end{bmatrix}^{\mathrm{T}}$ and*

$$\mathfrak{F}^{-1}\mathcal{L}_{\varsigma(t)}\mathfrak{F} = \begin{bmatrix}\bar{\boldsymbol{\nu}}_1 \\ \bar{\mathfrak{F}}\end{bmatrix}\mathcal{L}_{\varsigma(t)}\begin{bmatrix}\boldsymbol{\nu}_1 & \tilde{\mathfrak{F}}\end{bmatrix} = \begin{bmatrix}0 & \bar{\boldsymbol{\nu}}_1\mathcal{L}_{\varsigma(t)}\tilde{\mathfrak{F}} \\ 0 & \bar{\mathfrak{F}}\mathcal{L}_{\varsigma(t)}\tilde{\mathfrak{F}}\end{bmatrix}.$$

where $\bar{\boldsymbol{\nu}}_1 \in \mathbb{R}^{1\times\mathbf{N}}$ and $\bar{\mathfrak{F}} = \boldsymbol{col}(\bar{\boldsymbol{\nu}}_i)_{i=2}^{\mathbf{N}} \in \mathbb{R}^{(\mathbf{N}-1)\times\mathbf{N}}$. Accordingly, all eigenvalues of $\bar{\mathcal{L}}_{\varsigma(t)} = \bar{\mathfrak{F}}\mathcal{L}_{\varsigma(t)}\tilde{\mathfrak{F}}$ also have positive real parts, and $\bar{\mathcal{L}}_{\varsigma(t)}$ is nonsingular [16].

Remark 2. *The formation controller outlined in protocol (3) consists of three components.* $\mathbf{K}_1$ *is mainly used to adjust the dynamic behaviors of the formation reference, whereas* $\mathbf{K}_{2,\varsigma(t)}$ *and* $\boldsymbol{\alpha}$ *serve to steer the formation error toward zero over switching directed communication graphs. The relative coupling term only utilizes local information from neighboring agents, which can drive the formation error to converge to zero under switching directed topologies. The compensation signal* $\boldsymbol{c}_i(t)$ *is designed to counteract the impact induced by the derivative of the desired formation and further improve the feasibility of formation realization.*

Let $\boldsymbol{x}(t) = \mathbf{col}\big(\boldsymbol{x}_i(t)\big)_{i=1}^{\mathbf{N}}$ and $\boldsymbol{c}(t) = \mathbf{col}\big(\boldsymbol{c}_i(t)\big)_{i=1}^{\mathbf{N}}$. Then, with the formation control protocol (3), the closed-loop DN (1) can be formulated by

$$\begin{aligned}\dot{\boldsymbol{x}}(t) =&\big(\mathbf{I}_{\mathbf{N}} \otimes (\mathbf{A}+\mathbf{B}\mathbf{K}_1) - (\boldsymbol{\alpha}\mathcal{L}_{\varsigma(t)}) \otimes (\mathbf{B}\mathbf{K}_{2,\varsigma(t)})\big)\boldsymbol{x}(t)\\ &+\big((\boldsymbol{\alpha}\mathcal{L}_{\varsigma(t)}) \otimes (\mathbf{B}\mathbf{K}_{2,\varsigma(t)}) - \mathbf{I}_{\mathbf{N}} \otimes (\mathbf{B}\mathbf{K}_1)\big)\boldsymbol{y}(t) + (\mathbf{I}_{\mathbf{N}} \otimes \mathbf{B})\boldsymbol{c}(t).\end{aligned} \tag{4}$$

Define the formation error variable $\boldsymbol{\epsilon}_i(t) = \boldsymbol{x}_i(t) - \boldsymbol{y}_i(t)$ and $\boldsymbol{\epsilon}(t) = \mathbf{col}\big(\boldsymbol{\epsilon}_i(t)\big)_{i=1}^{\mathbf{N}}$. Then, system (4) can be rewritten as

$$\begin{aligned}\dot{\boldsymbol{\epsilon}}(t) =&\big(\mathbf{I}_{\mathbf{N}} \otimes (\mathbf{A}+\mathbf{B}\mathbf{K}_1) - (\boldsymbol{\alpha}\mathcal{L}_{\varsigma(t)}) \otimes (\mathbf{B}\mathbf{K}_{2,\varsigma(t)})\big)\boldsymbol{\epsilon}(t)\\ &+(\mathbf{I}_{\mathbf{N}} \otimes \mathbf{A})\boldsymbol{y}(t) - (\mathbf{I}_{\mathbf{N}} \otimes \mathbf{I}_{\mathbf{p}})\dot{\boldsymbol{y}}(t) + (\mathbf{I}_{\mathbf{N}} \otimes \mathbf{B})\boldsymbol{c}(t).\end{aligned} \tag{5}$$

Define $\boldsymbol{\xi}(t) = (\mathfrak{S}^{-1} \otimes \mathbf{I}_{\mathbf{p}})\boldsymbol{\epsilon}(t) = \mathbf{col}\big(\boldsymbol{\xi}_i(t)\big)_{i=1}^{\mathbf{N}}$ and $\mathbf{A}_c = \mathbf{A}+\mathbf{B}\mathbf{K}_1$. Then, from system (5), it is established that

$$\begin{aligned}\dot{\boldsymbol{\xi}}_1(t) =&\mathbf{A}_c\boldsymbol{\xi}_1(t) - \boldsymbol{\alpha}\big((\bar{\boldsymbol{\nu}}_1\mathcal{L}_{\varsigma(t)}\tilde{\mathfrak{S}}) \otimes (\mathbf{B}\mathbf{K}_{2,\varsigma(t)})\big)\bar{\boldsymbol{\xi}}(t)\\ &+(\bar{\boldsymbol{\nu}}_1 \otimes \mathbf{A})\boldsymbol{y}(t) - (\bar{\boldsymbol{\nu}}_1 \otimes \mathbf{I}_{\mathbf{p}})\dot{\boldsymbol{y}}(t) + (\bar{\boldsymbol{\nu}}_1 \otimes \mathbf{B})\boldsymbol{c}(t),\end{aligned} \tag{6}$$

and

$$\begin{aligned}\dot{\bar{\boldsymbol{\xi}}}(t) =&\big(\mathbf{I}_{\mathbf{N}-1} \otimes \mathbf{A}_c - (\boldsymbol{\alpha}\bar{\mathcal{L}}_{\varsigma(t)}) \otimes (\mathbf{B}\mathbf{K}_{2,\varsigma(t)})\big)\bar{\boldsymbol{\xi}}(t)\\ &+(\bar{\mathfrak{S}} \otimes \mathbf{A})\boldsymbol{y}(t) - (\bar{\mathfrak{S}} \otimes \mathbf{I}_{\mathbf{p}})\dot{\boldsymbol{y}}(t) + (\bar{\mathfrak{S}} \otimes \mathbf{B})\boldsymbol{c}(t),\end{aligned} \tag{7}$$

where $\bar{\boldsymbol{\xi}}(t) = \mathbf{col}\big(\xi_i(t)\big)_{i=2}^{\mathbf{N}} \in \mathbb{R}^{(\mathbf{N}-1)\mathbf{p}}$.

Before presenting the main conclusions of this research, several key definition and lemmas are introduced to support the following theoretical derivation.

Definition 2 ([21])**.** *Given positive constant satisfying* $\varsigma_1 < \infty$*, the switched signal* $\varsigma(t)$ *is defined to admit a dwell time restriction, provided that the interval between every two successive switching moments obeys* $t_{s+1} - t_s \geq \varsigma_1$ *for all* $s \in \mathbb{N}$.

Lemma 1. *The DN (4) under the formation control protocol (3) achieves the TVF associated with* $\boldsymbol{y}(t)$*, namely* $\lim_{t\to\infty}\big(\boldsymbol{x}(t) - \boldsymbol{y}(t) - \mathbf{1}_{\mathbf{N}}\otimes\boldsymbol{\xi}_1(t)\big) = 0$*, if and only if the following two conditions are satisfied:*

(I) for any $i \in \mathbb{S}_{[1,\mathbf{N}]}$*, and* $j \in \aleph^i_{\varsigma(t)}$*, it holds that*

$$\lim_{t\to\infty} \bar{\mathbf{B}}(\mathbf{A}\boldsymbol{y}_{ij}(t) - \dot{\boldsymbol{y}}_{ij}(t)) = 0, \tag{8}$$

(II) the following switched system exhibits asymptotic convergence:

$$\dot{\tilde{\boldsymbol{\xi}}}(t) = \big(\mathbf{I}_{\mathbf{N}-1} \otimes \mathbf{A}_c - (\boldsymbol{\alpha}\bar{\mathcal{L}}_{\varsigma(t)}) \otimes (\mathbf{B}\mathbf{K}_{2,\varsigma(t)})\big)\tilde{\boldsymbol{\xi}}(t), \tag{9}$$

where $\boldsymbol{y}_{ij}(t) = \boldsymbol{y}_i(t) - \boldsymbol{y}_j(t)$*,* $\bar{\mathbf{B}} \in \mathbb{R}^{(\mathbf{p}-\mathbf{q})\times\mathbf{p}}$ *and* $\bar{\mathbf{B}}\mathbf{B} = \mathbf{0}$.

Remark 3. *The proof of Lemma 1 follows directly from the derivations presented in [16]. The condition (8) serves as a feasibility condition for the prescribed time-varying formation, which verifies whether the relative formation signals can be realized via each node's dynamics and the channels characterized by* $\mathbf{B}$*. After this feasibility condition is fulfilled, the remaining task is to design the formation control protocol (3) and the switching rule* $\varsigma(t)$ *to guarantee the stability of the reduced formation error system (9). As such, condition (8) builds a bridge between the predefined time-varying formation pattern and the subsequent control protocol design. From* $\bar{\mathbf{B}}\mathbf{B} = 0$*, it can be verified that*

$$\lim_{t\to\infty}\big(\bar{\mathbf{B}}\mathbf{A}\boldsymbol{y}_{ij}(t)-\bar{\mathbf{B}}\dot{\boldsymbol{y}}_{ij}(t)+\bar{\mathbf{B}}\mathbf{B}(\boldsymbol{c}_i(t)-\boldsymbol{c}_j(t))\big)=0.$$

Also, we can determine $\boldsymbol{c}_i(t)$ *and* $\boldsymbol{c}_j(t)$ *such that*

$$\lim_{t\to\infty}\big(\tilde{\mathbf{B}}\mathbf{A}\boldsymbol{y}_{ij}(t)-\tilde{\mathbf{B}}\dot{\boldsymbol{y}}_{ij}(t)+(\boldsymbol{c}_i(t)-\boldsymbol{c}_j(t))\big)=0,$$

where $\tilde{\mathbf{B}}\in\mathbb{R}^{\mathbf{q}\times\mathbf{p}}$, $\tilde{\mathbf{B}}\mathbf{B}=\mathbf{I}_{\mathbf{q}}$ *and* $\boldsymbol{col}(\tilde{\mathbf{B}},\bar{\mathbf{B}})$ *is nonsingular. Then, it can be calculated that* $\lim_{t\to\infty}\big(\mathbf{A}\boldsymbol{y}_{ij}(t)-\dot{\boldsymbol{y}}_{ij}(t)+\mathbf{B}\boldsymbol{c}_{ij}(t)\big)=0$, *and thus* $\lim_{t\to\infty}\big((\bar{\mathfrak{F}}\otimes\mathbf{A})\boldsymbol{y}(t)-(\bar{\mathfrak{F}}\otimes\mathbf{I}_{\mathbf{p}})\dot{\boldsymbol{y}}(t)+(\bar{\mathfrak{F}}\otimes\mathbf{B})\boldsymbol{c}(t)\big)=0$. *Hence, it follows from* (7) *and Lemma 1 that the distributed formation control of the DN* (1) *is accordingly transformed into the asymptotic stability verification of the switched system* (9). *Accordingly, the formation compensation signal* $\boldsymbol{c}_i(t)$ *can be designated as* $\boldsymbol{c}_i(t)=-\tilde{\mathbf{B}}\big(\mathbf{A}\boldsymbol{y}_i(t)-\dot{\boldsymbol{y}}_i(t)\big)$ *for any* $i\in\mathbb{S}_{[1,\mathbf{N}]}$.

Remark 4. *Following Lemma 1 and the nonsingular coordinate transformation* $\boldsymbol{\xi}(t)=(\mathfrak{F}^{-1}\otimes\mathbf{I}_{\mathbf{p}})\boldsymbol{\epsilon}(t)$, *an explicit expression of the formation reference function* $\boldsymbol{\hbar}(t)$ *can be provided by* $\boldsymbol{\hbar}(t)=(\bar{\boldsymbol{\nu}}_1\otimes\mathbf{I}_{\mathbf{p}})\big(\boldsymbol{x}(t)-\boldsymbol{y}(t)\big)$, *which captures macroscopic motion across the entire TVF. Particularly, the considered TVF problem degenerates into a consensus problem when* $\boldsymbol{y}(t)\equiv 0$. *In this scenario,* $\boldsymbol{\hbar}(t)$ *serves as the consensus function associated with the DNs. As a consequence, it is observed from Equation* (6) *that the macroscopic motion of the overall formation is simultaneously governed by node dynamics, switching communication topologies, compensation signal* $\boldsymbol{c}(t)$, *and prescribed formation geometry.*

Lemma 2 ([22]). *For the directed graph* $\mathcal{G}_{\varsigma(t)}$ *containing a spanning tree and the structure of* $\bar{\mathcal{L}}_{\varsigma(t)}=\bar{\mathfrak{F}}\mathcal{L}_{\varsigma(t)}\tilde{\mathfrak{F}}$, *there exists a positive scalar* $\boldsymbol{\gamma}_{\varsigma(t)}<\min\big\{\mathbf{Re}\big(\boldsymbol{\lambda}_i(\bar{\mathcal{L}}_{\varsigma(t)}\big),\ i\in\mathbb{S}_{[1,\mathbf{N}-1]}\big\}$ *and the symmetric positive definite matrix* $\wp_{\varsigma(t)}\in\mathbb{R}^{(\mathbf{N}-1)\times(\mathbf{N}-1)}$ *such that*

$$\bar{\mathcal{L}}^{\mathrm{T}}_{\varsigma(t)}\wp_{\varsigma(t)}+\wp_{\varsigma(t)}\bar{\mathcal{L}}_{\varsigma(t)}>2\boldsymbol{\gamma}_{\varsigma(t)}\wp_{\varsigma(t)}. \tag{10}$$

Remark 5. *Lemma 2 is mainly employed to handle the asymmetric nature of directed Laplacian matrix. Even though* $\bar{\mathcal{L}}_{\varsigma(t)}$ *is typically non-symmetric and can admit complex eigenvalues, inequality* (10) *yields a positive definite weighting matrix* $\wp_{\varsigma(t)}$, *which facilitates the construction of the TDTVLF.*

Lemma 3 ([23]). *For any vectors* $\boldsymbol{y}_1$ *and* $\boldsymbol{y}_2$, *and the symmetric positive definite matrix* $\mathbf{H}$ *with appropriate dimension, the following inequality holds:*

$$\pm 2\boldsymbol{y}_1^{\mathrm{T}}\boldsymbol{y}_2\le\boldsymbol{y}_1^{\mathrm{T}}\mathbf{H}\boldsymbol{y}_1+\boldsymbol{y}_2^{\mathrm{T}}\mathbf{H}^{-1}\boldsymbol{y}_2. \tag{11}$$

Lemma 4 ([24]). *Consider the symmetric matrices* $\mathbf{M}_1>0$ *and* $\mathbf{M}_2$. *Then, for any vector* $\boldsymbol{x}$ *with appropriate dimension, we have*

$$\boldsymbol{\lambda}_{\min}\big(\mathbf{M}_1^{-1}\mathbf{M}_2\big)\boldsymbol{x}^{\mathrm{T}}\mathbf{M}_1\boldsymbol{x}\le\boldsymbol{x}^{\mathrm{T}}\mathbf{M}_2\boldsymbol{x}\le\boldsymbol{\lambda}_{\max}\big(\mathbf{M}_1^{-1}\mathbf{M}_2\big)\boldsymbol{x}^{\mathrm{T}}\mathbf{M}_1\boldsymbol{x}. \tag{12}$$

Lemma 5. *For the symmetric positive-definite matrix* $\wp_{\varsigma(t)}$ *and symmetric matrix* $\mathscr{A}=(\mathscr{A}_{ij})_{\Psi\times\Psi}$ *and* $i,j\in\mathbb{S}_{[1,\Psi]}$, *there exists a nonsingular matrix* $\boldsymbol{\Omega}_{\Psi}$ *such that*

$$\mathscr{A}_{\wp_{\varsigma(t)}}=\begin{bmatrix}\wp_{\varsigma(t)}\otimes\mathscr{A}_{11} & * & \cdots & *\\ \wp_{\varsigma(t)}\otimes\mathscr{A}_{21} & \wp_{\varsigma(t)}\otimes\mathscr{A}_{22} & \cdots & *\\ \vdots & \vdots & \ddots & \vdots\\ \wp_{\varsigma(t)}\otimes\mathscr{A}_{\Psi 1} & \wp_{\varsigma(t)}\otimes\mathscr{A}_{\Psi 2} & \cdots & \wp_{\varsigma(t)}\otimes\mathscr{A}_{\Psi\Psi}\end{bmatrix}=\boldsymbol{\Omega}_{\Psi}(\wp_{\varsigma(t)}\otimes\mathscr{A})\boldsymbol{\Omega}_{\Psi}^{\mathrm{T}} \tag{13}$$

where $\boldsymbol{\Omega}_{\Psi}$ *is expressed as*

$$\boldsymbol{\Omega}_{\Psi}=\boldsymbol{col}(\boldsymbol{\pi}_1,\ \boldsymbol{\pi}_{1+\Psi},\ \cdots,\ \boldsymbol{\pi}_{1+(\mathbf{N}-2)\Psi},\ \boldsymbol{\pi}_2,\ \boldsymbol{\pi}_{2+\Psi},\ \cdots,\ \boldsymbol{\pi}_{2+(\mathbf{N}-2)\Psi},\ \cdots,\ \boldsymbol{\pi}_{\Psi},\ \boldsymbol{\pi}_{2\Psi},\ \cdots,\ \boldsymbol{\pi}_{(\mathbf{N}-1)\Psi}),$$

with $\boldsymbol{\pi}_m=\big[\mathbf{0}_{\mathbf{p}\times(m-1)\mathbf{p}}\ \ \mathbf{I}_{\mathbf{p}}\ \ \mathbf{0}_{\mathbf{p}\times((\mathbf{N}-1)\Psi-m)\mathbf{p}}\big]$ *and* $m\in\mathbb{S}_{[1,(\mathbf{N}-1)\Psi]}$.

Remark 6. *Given that the directed graph* $\mathcal{G}_{\varsigma(t)}$ *containing a spanning tree and with the introduction of the nonsingular matrix* $\tilde{\mathfrak{F}}$, *the reduced formation error system* (9) *is acquired. As a result, and all eigenvalues of*

$\bar{\mathcal{L}}_{\varsigma(t)} = \tilde{\mathfrak{S}}\mathcal{L}_{\varsigma(t)}\tilde{\mathfrak{S}}$ *possess positive real parts. Meanwhile, and there exists a symmetric positive-definite matrix* $\wp_{\varsigma(t)} \in \mathbb{R}^{(\mathbf{N}-1)\times(\mathbf{N}-1)}$ *such that inequality* (10) *holds. Taking all these factors into account, we propose the property of Kronecker product decoupling in formula* (13)*. The proof of Lemma 5 shares similar technical arguments with the one presented in [25,26], and thus is omitted for brevity. Since* $\mathbf{\Omega}_{\mathbf{\Psi}}$ *is nonsingular, Equation* (13) *establishes an equivalence between the negative-definite condition of the high-dimensional matrix* $\mathscr{A}_{\wp_{\varsigma(t)}}$ *and that for its low-dimensional counterpart* $\mathscr{A}$*. This particular Kronecker product feature allows us to construct a synchronization criterion independent of the network node scale* $\mathbf{N}$*. Consequently, the resulting criterion is applicable to formation control over large-scale DNs.*

3. Main Results

In this section, a TVF control criterion is established for the DN (1) under switching topologies, by constructing a TDTVLF approach.

Theorem 1. *For the prescribed the TVF* $\boldsymbol{y}(t)$ *satisfying the constraint* (8)*, suppose that there exists positive scalars* $\boldsymbol{\eta}_k$*,* $\boldsymbol{\beta}$*,* $\boldsymbol{\mu} \geq 1$*, and symmetric positive matrices* $\mathbf{P}_{k,a} \in \mathbb{R}^{\mathbf{p}\times\mathbf{p}}$*,* $\mathbf{Q}_k \in \mathbb{R}^{\mathbf{p}\times\mathbf{p}}$*,* $\mathbf{R}_k \in \mathbb{R}^{\mathbf{p}\times\mathbf{p}}$*,* $\mathbf{Z}_k \in \mathbb{R}^{\mathbf{q}\times\mathbf{q}}$*,* $k \in \aleph$*,* $a \in \mathbb{S}_{[1,2]}$*, such that*

$$\begin{bmatrix} \mathbf{\Theta}_{11}^k & * & * \\ \mathbf{\Theta}_{12}^k & \bar{\mathbf{R}}_k - 2\boldsymbol{\eta}_k\bar{\mathbf{Q}}_k & * \\ \boldsymbol{\eta}_k\boldsymbol{\alpha}\sqrt{\boldsymbol{\varkappa}_{k,2}}\mathbf{B}\mathbf{Z}_k\mathbf{B}^{\mathrm{T}} & \mathbf{0} & -\bar{\mathbf{R}}_k \end{bmatrix} < 0, \tag{14}$$

$$\begin{bmatrix} \hat{\mathbf{\Theta}}_{11}^k & * & * \\ \hat{\mathbf{\Theta}}_{12}^k & \bar{\mathbf{R}}_k - 2\boldsymbol{\eta}_k\bar{\mathbf{Q}}_k & * \\ \boldsymbol{\eta}_k\boldsymbol{\alpha}\sqrt{\boldsymbol{\varkappa}_{k,2}}\mathbf{B}\mathbf{Z}_k\mathbf{B}^{\mathrm{T}} & \mathbf{0} & -\bar{\mathbf{R}}_k \end{bmatrix} < 0, \tag{15}$$

$$\begin{bmatrix} \boldsymbol{\psi}_{k,2} & * & * \\ \hat{\mathbf{\Theta}}_{12}^k & \bar{\mathbf{R}}_k - 2\boldsymbol{\eta}_k\bar{\mathbf{Q}}_k & * \\ \boldsymbol{\eta}_k\boldsymbol{\alpha}\sqrt{\boldsymbol{\varkappa}_{k,2}}\mathbf{B}\mathbf{Z}_k\mathbf{B}^{\mathrm{T}} & \mathbf{0} & -\bar{\mathbf{R}}_k \end{bmatrix} < 0, \tag{16}$$

$$\mathbf{P}_{k,1} \leq \boldsymbol{\mu}\mathbf{P}_{r,2},\ \boldsymbol{\mu}\boldsymbol{\tau} > 1,\ k \neq r \in \aleph, \tag{17}$$

where $\bar{\mathbf{Q}}_k = \mathbf{Q}_k^{-1}$ *and*

$$\begin{aligned}
&\mathbf{\Theta}_{11}^k = \frac{\bar{\mathbf{P}}_{k,2} - \bar{\mathbf{P}}_{k,1}}{\varsigma_1} + \boldsymbol{\psi}_{k,1}, \mathbf{\Theta}_{12}^k = \bar{\mathbf{P}}_{k,1} + \boldsymbol{\eta}_k\mathbf{A}_c\bar{\mathbf{Q}}_k^{\mathrm{T}} - \bar{\mathbf{Q}}_k, \\
&\hat{\mathbf{\Theta}}_{11}^k = \frac{\bar{\mathbf{P}}_{k,2} - \bar{\mathbf{P}}_{k,1}}{\varsigma_1} + \boldsymbol{\psi}_{k,2}, \hat{\mathbf{\Theta}}_{12}^k = \bar{\mathbf{P}}_{k,2} + \boldsymbol{\eta}_k\mathbf{A}_c\bar{\mathbf{Q}}_k^{\mathrm{T}} - \bar{\mathbf{Q}}_k, \\
&\boldsymbol{\psi}_{k,a} = \boldsymbol{Sym}(\mathbf{A}_c\bar{\mathbf{Q}}_k) - \boldsymbol{\alpha}\boldsymbol{\varkappa}_{k,1}\mathbf{B}\mathbf{Z}_k\mathbf{B}^{\mathrm{T}} + \boldsymbol{\beta}\bar{\mathbf{P}}_{k,a},\ \bar{\mathbf{P}}_{k,1} = \bar{\mathbf{Q}}_k\mathbf{P}_{k,1}\bar{\mathbf{Q}}_k^{\mathrm{T}}, \\
&\boldsymbol{\varkappa}_{k,1} = \boldsymbol{\lambda}_{\min}\big(\bar{\mathcal{L}}_k + \wp_k^{-1}\bar{\mathcal{L}}_k^{\mathrm{T}}\wp_k\big),\ \bar{\mathbf{P}}_{k,2} = \bar{\mathbf{Q}}_k\mathbf{P}_{k,2}\bar{\mathbf{Q}}_k^{\mathrm{T}}, \\
&\boldsymbol{\varkappa}_{k,2} = \boldsymbol{\lambda}_{\max}\big(\wp_k^{-1}\bar{\mathcal{L}}_k^{\mathrm{T}}\wp_k\bar{\mathcal{L}}_k\big),\ \bar{\mathbf{R}}_k = \bar{\mathbf{Q}}_k\mathbf{R}_k\bar{\mathbf{Q}}_k^{\mathrm{T}}.
\end{aligned}$$

Then, under the controller gain formulated by $\mathbf{K}_{2,k} = \mathbf{Z}_k\mathbf{B}^{\mathrm{T}}\mathbf{Q}_k^{\mathrm{T}}$ *and the dwell-time constraint*

$$\varsigma_1 > \frac{\ln(\boldsymbol{\mu}\boldsymbol{\tau})}{\boldsymbol{\beta}},\quad \boldsymbol{\tau} = \max\big\{\boldsymbol{\lambda}_{\max}\big(\wp_r^{-1}\wp_k\big), k \neq r \in \aleph\big\}, \tag{18}$$

system (9) *exhibits exponential stability, while the DN* (1) *attains the prescribed TVF* $\boldsymbol{y}(t)$*.*

Proof. For any switching interval $[t_s, t_{s+1})$, define $\varsigma(t) = k$ with $k \in \aleph$. Given system (9), construct the following TDTVLF:

$$\mathbf{V}(t) = \mathbf{V}_k\big(\tilde{\boldsymbol{\xi}}(t)\big) = \tilde{\boldsymbol{\xi}}^{\mathrm{T}}(t)\big(\wp_k \otimes \mathbf{P}_k(t)\big)\tilde{\boldsymbol{\xi}}(t), \tag{19}$$

with the time-varying matrix taking the form of

$$\mathbf{P}_k(t) = \begin{cases} \frac{t_s+\varsigma_1-t}{\varsigma_1}\mathbf{P}_{k,1} + \big(1 - \frac{t_s+\varsigma_1-t}{\varsigma_1}\big)\mathbf{P}_{k,2}, & t \in [t_s, t_s+\varsigma_1), \\ \mathbf{P}_{k,2}, & t \in [t_s+\varsigma_1, t_{s+1}). \end{cases} \tag{20}$$

For $t \in [t_s, t_s+\varsigma_1)$, taking the derivative of $\mathbf{V}(t)$ along the trajectory of (9) gives

$$\begin{aligned}\dot{\mathbf{V}}(t)+\boldsymbol{\beta}\mathbf{V}(t)=&\,2\frac{t_s+\varsigma_1-t}{\varsigma_1}\tilde{\boldsymbol{\xi}}^{\mathrm{T}}(t)\big(\wp_k\otimes\mathbf{P}_{k,1}\big)\dot{\tilde{\boldsymbol{\xi}}}(t)\\&+2\Big(1-\frac{t_s+\varsigma_1-t}{\varsigma_1}\Big)\tilde{\boldsymbol{\xi}}^{\mathrm{T}}(t)\big(\wp_k\otimes\mathbf{P}_{k,2}\big)\dot{\tilde{\boldsymbol{\xi}}}(t)\\&+\frac{t_s+\varsigma_1-t}{\varsigma_1}\tilde{\boldsymbol{\xi}}^{\mathrm{T}}(t)\bigg(\wp_k\otimes\Big(\frac{\mathbf{P}_{k,2}-\mathbf{P}_{k,1}}{\varsigma_1}+\boldsymbol{\beta}\mathbf{P}_{k,1}\Big)\bigg)\tilde{\boldsymbol{\xi}}(t)\\&+\Big(1-\frac{t_s+\varsigma_1-t}{\varsigma_1}\Big)\tilde{\boldsymbol{\xi}}^{\mathrm{T}}(t)\bigg(\wp_k\otimes\Big(\frac{\mathbf{P}_{k,2}-\mathbf{P}_{k,1}}{\varsigma_1}+\boldsymbol{\beta}\mathbf{P}_{k,2}\Big)\bigg)\tilde{\boldsymbol{\xi}}(t).\end{aligned}\tag{21}$$

By using the system Equation (9), there exists symmetric positive matrix $\mathbf{Q}_k$ and positive scalar $\boldsymbol{\eta}_k$ such that

$$2\big[\tilde{\boldsymbol{\xi}}^{\mathrm{T}}(t)(\wp_k\otimes\mathbf{Q}_k)+\boldsymbol{\eta}_k\dot{\tilde{\boldsymbol{\xi}}}^{\mathrm{T}}(t)(\wp_k\otimes\mathbf{Q}_k)\big]\big[(\mathbf{I}_{\mathbf{N}-1}\otimes\mathbf{A}_c)\tilde{\boldsymbol{\xi}}(t)-\boldsymbol{\alpha}\big(\bar{\mathcal{L}}_k\otimes(\mathbf{B}\mathbf{K}_{2,k})\big)\tilde{\boldsymbol{\xi}}(t)-\dot{\tilde{\boldsymbol{\xi}}}(t)\big]=0,\tag{22}$$

which implies that

$$\begin{aligned}&2\tilde{\boldsymbol{\xi}}^{\mathrm{T}}(t)\big(\wp_k\otimes(\mathbf{Q}_k\mathbf{A}_c)\big)\tilde{\boldsymbol{\xi}}(t)-2\tilde{\boldsymbol{\xi}}^{\mathrm{T}}(t)(\wp_k\otimes\mathbf{Q}_k)\dot{\tilde{\boldsymbol{\xi}}}(t)-2\boldsymbol{\alpha}\tilde{\boldsymbol{\xi}}^{\mathrm{T}}(t)\\&\times\big((\wp_k\bar{\mathcal{L}}_k)\otimes(\mathbf{Q}_k\mathbf{B}\mathbf{K}_{2,k})\big)\tilde{\boldsymbol{\xi}}(t)+2\boldsymbol{\eta}_k\dot{\tilde{\boldsymbol{\xi}}}^{\mathrm{T}}(t)\big(\wp_k\otimes(\mathbf{Q}_k\mathbf{A}_c)\big)\tilde{\boldsymbol{\xi}}(t)-2\boldsymbol{\eta}_k\boldsymbol{\alpha}\\&\times\dot{\tilde{\boldsymbol{\xi}}}^{\mathrm{T}}(t)\big((\wp_k\bar{\mathcal{L}}_k)\otimes(\mathbf{Q}_k\mathbf{B}\mathbf{K}_{2,k})\big)\tilde{\boldsymbol{\xi}}(t)-2\boldsymbol{\eta}_k\dot{\tilde{\boldsymbol{\xi}}}^{\mathrm{T}}(t)(\wp_k\otimes\mathbf{Q}_k)\dot{\tilde{\boldsymbol{\xi}}}(t)=0.\end{aligned}\tag{23}$$

Notice that $\mathbf{K}_{2,k}=\mathbf{Z}_k\mathbf{B}^{\mathrm{T}}\mathbf{Q}_k^{\mathrm{T}}$ and the matrix $\mathbf{Q}_k\mathbf{B}\mathbf{Z}_k\mathbf{B}^{\mathrm{T}}\mathbf{Q}_k^{\mathrm{T}}$ is semi-positive definite. Then, for the symmetric positive matrix $\mathbf{Q}_k$, we can conclude that

$$\begin{aligned}&-2\boldsymbol{\alpha}\tilde{\boldsymbol{\xi}}^{\mathrm{T}}(t)\big((\wp_k\bar{\mathcal{L}}_k)\otimes(\mathbf{Q}_k\mathbf{B}\mathbf{K}_{2,k})\big)\tilde{\boldsymbol{\xi}}(t)\\&=-2\boldsymbol{\alpha}\tilde{\boldsymbol{\xi}}^{\mathrm{T}}(t)\big((\wp_k\bar{\mathcal{L}}_k)\otimes(\mathbf{Q}_k\mathbf{B}\mathbf{Z}_k\mathbf{B}^{\mathrm{T}}\mathbf{Q}_k^{\mathrm{T}})\big)\tilde{\boldsymbol{\xi}}(t)\\&=-\boldsymbol{\alpha}\tilde{\boldsymbol{\xi}}^{\mathrm{T}}(t)\big((\wp_k\bar{\mathcal{L}}_k+\bar{\mathcal{L}}_k^{\mathrm{T}}\wp_k)\otimes(\mathbf{Q}_k\mathbf{B}\mathbf{K}_{2,k})\big)\tilde{\xi}(t)\\&\le-\boldsymbol{\alpha}\boldsymbol{\varkappa}_{k,1}\tilde{\boldsymbol{\xi}}^{\mathrm{T}}(t)\big(\wp_k\otimes(\mathbf{Q}_k\mathbf{B}\mathbf{Z}_k\mathbf{B}^{\mathrm{T}}\mathbf{Q}_k^{\mathrm{T}})\big)\tilde{\boldsymbol{\xi}}(t).\end{aligned}\tag{24}$$

Similarly, for any symmetric positive definite matrix $\mathbf{R}_k$, applying Lemmas 2 and 3 yields

$$\begin{aligned}&-2\boldsymbol{\eta}_k\boldsymbol{\alpha}\dot{\tilde{\xi}}^{\mathrm{T}}(t)\big((\wp_k\bar{\mathcal{L}}_k)\otimes(\mathbf{Q}_k\mathbf{B}\mathbf{Z}_k\mathbf{B}^{\mathrm{T}}\mathbf{Q}_k^{\mathrm{T}})\big)\tilde{\boldsymbol{\xi}}(t)\\&\le\dot{\tilde{\boldsymbol{\xi}}}^{\mathrm{T}}(t)\big(\wp_k\otimes\mathbf{R}_k\big)\dot{\tilde{\boldsymbol{\xi}}}(t)+\boldsymbol{\alpha}^2\boldsymbol{\eta}_k^2\tilde{\boldsymbol{\xi}}^{\mathrm{T}}(t)\big((\wp_k\bar{\mathcal{L}}_k)^{\mathrm{T}}\\&\otimes(\mathbf{Q}_k\mathbf{B}\mathbf{Z}_k\mathbf{B}^{\mathrm{T}}\mathbf{Q}_k^{\mathrm{T}})\big)\big(\wp_k^{-1}\otimes\mathbf{R}_k^{-1}\big)\big((\wp_k\bar{\mathcal{L}}_k)\otimes(\mathbf{Q}_k\mathbf{B}\mathbf{Z}_k\mathbf{B}^{\mathrm{T}}\mathbf{Q}_k^{\mathrm{T}})\big)\tilde{\boldsymbol{\xi}}(t)\\&=\dot{\tilde{\boldsymbol{\xi}}}^{\mathrm{T}}(t)\big(\wp_k\otimes\mathbf{R}_k\big)\dot{\tilde{\boldsymbol{\xi}}}(t)+\boldsymbol{\alpha}^2\boldsymbol{\eta}_k^2\tilde{\boldsymbol{\xi}}^{\mathrm{T}}(t)\big((\bar{\mathcal{L}}_k^{\mathrm{T}}\wp_k\bar{\mathcal{L}}_k)\otimes(\boldsymbol{\Gamma}_k\mathbf{R}_k^{-1}\boldsymbol{\Gamma}_k)\big)\tilde{\boldsymbol{\xi}}(t)\\&\le\dot{\tilde{\boldsymbol{\xi}}}^{\mathrm{T}}(t)\big(\wp_k\otimes\mathbf{R}_k\big)\dot{\tilde{\boldsymbol{\xi}}}(t)+\boldsymbol{\alpha}^2\boldsymbol{\eta}_k^2\boldsymbol{\lambda}_{\max}\big(\wp_k^{-1}(\bar{\mathcal{L}}_k^{\mathrm{T}}\wp_k\bar{\mathcal{L}}_k)\big)\\&\times\tilde{\boldsymbol{\xi}}^{\mathrm{T}}(t)\big(\wp_k\otimes(\boldsymbol{\Gamma}_k\mathbf{R}_k^{-1}\boldsymbol{\Gamma}_k)\big)\tilde{\boldsymbol{\xi}}(t),\end{aligned}\tag{25}$$

where $\boldsymbol{\Gamma}_k=\mathbf{Q}_k\mathbf{B}\mathbf{Z}_k\mathbf{B}^{\mathrm{T}}\mathbf{Q}_k^{\mathrm{T}}$.

Thus, utilizing the formulas (21)–(25) gives

$$\begin{aligned}\dot{\mathbf{V}}(t)+\boldsymbol{\beta}\mathbf{V}(t)\le&\,\frac{t_s+\varsigma_1-t}{\varsigma_1}\bigg[2\tilde{\boldsymbol{\xi}}^{\mathrm{T}}(t)\big(\wp_k\otimes\mathbf{P}_{k,1}\big)\dot{\tilde{\boldsymbol{\xi}}}(t)\\&+\tilde{\boldsymbol{\xi}}^{\mathrm{T}}(t)\bigg(\wp_k\otimes\Big(\frac{\mathbf{P}_{k,2}-\mathbf{P}_{k,1}}{\varsigma_1}+\boldsymbol{\beta}\mathbf{P}_{k,1}\Big)\bigg)\tilde{\boldsymbol{\xi}}(t)\bigg]\\&+\Big(1-\frac{t_s+\varsigma_1-t}{\varsigma_1}\Big)\bigg[2\tilde{\boldsymbol{\xi}}^{\mathrm{T}}(t)\big(\wp_k\otimes\mathbf{P}_{k,2}\big)\dot{\tilde{\boldsymbol{\xi}}}(t)\\&+\tilde{\boldsymbol{\xi}}^{\mathrm{T}}(t)\bigg(\wp_k\otimes\Big(\frac{\mathbf{P}_{k,2}-\mathbf{P}_{k,1}}{\varsigma_1}+\boldsymbol{\beta}\mathbf{P}_{k,2}\Big)\bigg)\tilde{\boldsymbol{\xi}}(t)\bigg]\\&+2\tilde{\boldsymbol{\xi}}^{\mathrm{T}}(t)\big(\wp_k\otimes(\mathbf{Q}_k\mathbf{A}_c)\big)\tilde{\boldsymbol{\xi}}(t)-2\tilde{\boldsymbol{\xi}}^{\mathrm{T}}(t)(\wp_k\otimes\mathbf{Q}_k)\dot{\tilde{\boldsymbol{\xi}}}(t)\\&+2\boldsymbol{\eta}_k\dot{\tilde{\boldsymbol{\xi}}}^{\mathrm{T}}(t)\big(\wp_k\otimes(\mathbf{Q}_k\mathbf{A}_c)\big)\tilde{\boldsymbol{\xi}}(t)-2\boldsymbol{\eta}_k\dot{\tilde{\boldsymbol{\xi}}}^{\mathrm{T}}(t)(\wp_k\otimes\mathbf{Q}_k)\dot{\tilde{\boldsymbol{\xi}}}(t)\\&-\boldsymbol{\alpha}\boldsymbol{\varkappa}_{k,1}\tilde{\boldsymbol{\xi}}^{\mathrm{T}}(t)(\wp_k\otimes\boldsymbol{\Gamma}_k)\tilde{\boldsymbol{\xi}}(t)+\dot{\tilde{\boldsymbol{\xi}}}^{\mathrm{T}}(t)\big(\wp_k\otimes\mathbf{R}_k\big)\dot{\tilde{\boldsymbol{\xi}}}(t)\\&+\boldsymbol{\alpha}^2\boldsymbol{\eta}_k^2\boldsymbol{\varkappa}_{k,2}\tilde{\boldsymbol{\xi}}^{\mathrm{T}}(t)\big(\wp_k\otimes(\boldsymbol{\Gamma}_k\mathbf{R}_k^{-1}\boldsymbol{\Gamma}_k)\big)\tilde{\boldsymbol{\xi}}(t).\end{aligned}\tag{26}$$

Let $\boldsymbol{\nabla} = \mathbf{diag}(\mathbf{Q}_k, \mathbf{Q}_k)$, $\boldsymbol{\Upsilon}_k = \mathbf{col}\big(\tilde{\boldsymbol{\xi}}(t), \dot{\tilde{\boldsymbol{\xi}}}(t)\big)$, and

$$\begin{aligned}
\boldsymbol{\Theta}_{k,1} &= \begin{bmatrix} \boldsymbol{\Theta}_{11}^k + \boldsymbol{\alpha}^2\boldsymbol{\eta}_k^2\boldsymbol{\varkappa}_{k,2}\mathbf{B}\mathbf{Z}_k\mathbf{B}^{\mathrm{T}}\mathbf{Q}_k^{\mathrm{T}}\mathbf{R}_k^{-1}\mathbf{Q}_k\mathbf{B}\mathbf{Z}_k\mathbf{B}^{\mathrm{T}} & * \\ \boldsymbol{\Theta}_{12}^k & \bar{\mathbf{R}}_k - 2\boldsymbol{\eta}_k\bar{\mathbf{Q}}_k \end{bmatrix}, \\
\boldsymbol{\Theta}_{k,2} &= \begin{bmatrix} \hat{\boldsymbol{\Theta}}_{11}^k + \boldsymbol{\alpha}^2\boldsymbol{\eta}_k^2\boldsymbol{\varkappa}_{k,2}\mathbf{B}\mathbf{Z}_k\mathbf{B}^{\mathrm{T}}\mathbf{Q}_k^{\mathrm{T}}\mathbf{R}_k^{-1}\mathbf{Q}_k\mathbf{B}\mathbf{Z}_k\mathbf{B}^{\mathrm{T}} & * \\ \hat{\boldsymbol{\Theta}}_{12}^k & \bar{\mathbf{R}}_k - 2\boldsymbol{\eta}_k\bar{\mathbf{Q}}_k \end{bmatrix}, \\
\boldsymbol{\Theta}_{k,3} &= \begin{bmatrix} \boldsymbol{\psi}_{k,2} + \boldsymbol{\alpha}^2\boldsymbol{\eta}_k^2\boldsymbol{\varkappa}_{k,2}\mathbf{B}\mathbf{Z}_k\mathbf{B}^{\mathrm{T}}\mathbf{Q}_k^{\mathrm{T}}\mathbf{R}_k^{-1}\mathbf{Q}_k\mathbf{B}\mathbf{Z}_k\mathbf{B}^{\mathrm{T}} & * \\ \hat{\boldsymbol{\Theta}}_{12}^k & \bar{\mathbf{R}}_k - 2\boldsymbol{\eta}_k\bar{\mathbf{Q}}_k \end{bmatrix}.
\end{aligned} \tag{27}$$

Then, recalling inequalities (19)–(26) gives rise to

$$\begin{aligned}
\dot{\mathbf{V}}(t) + \boldsymbol{\beta}\mathbf{V}(t) \leq{}& \frac{t_s + \boldsymbol{\varsigma}_1 - t}{\boldsymbol{\varsigma}_1}\boldsymbol{\Upsilon}_k^{\mathrm{T}}\Big[\boldsymbol{\Omega}_2\big(\boldsymbol{\wp}_k \otimes (\boldsymbol{\nabla}\boldsymbol{\Theta}_{k,1}\boldsymbol{\nabla}^{\mathrm{T}})\big)\boldsymbol{\Omega}_2^{\mathrm{T}}\Big]\boldsymbol{\Upsilon}_k \\
&+ \Big(1 - \frac{t_s + \boldsymbol{\varsigma}_1 - t}{\boldsymbol{\varsigma}_1}\Big)\boldsymbol{\Upsilon}_k^{\mathrm{T}}\Big[\boldsymbol{\Omega}_2\big(\boldsymbol{\wp}_k \otimes (\boldsymbol{\nabla}\boldsymbol{\Theta}_{k,2}\boldsymbol{\nabla}^{\mathrm{T}})\big)\boldsymbol{\Omega}_2^{\mathrm{T}}\Big]\boldsymbol{\Upsilon}_k
\end{aligned} \tag{28}$$

where $\boldsymbol{\Omega}_2 = \mathbf{col}(\boldsymbol{\pi}_1, \boldsymbol{\pi}_3, \cdots, \boldsymbol{\pi}_{2\mathbf{N}-3}, \boldsymbol{\pi}_2, \boldsymbol{\pi}_4, \cdots, \boldsymbol{\pi}_{2\mathbf{N}-2})$ with $\boldsymbol{\pi}_m$ defined in Lemma 5 for $m \in \mathbb{S}_{[1,2(\mathbf{N}-1)]}$.

Similarly, for $t \in [t_s + \boldsymbol{\varsigma}_1, t_{s+1})$, repeating steps (21)–(26) results in

$$\dot{\mathbf{V}}(t) + \boldsymbol{\beta}\mathbf{V}(t) \leq \boldsymbol{\Upsilon}_k^{\mathrm{T}}\Big[\boldsymbol{\Omega}_2\big(\boldsymbol{\wp}_k \otimes (\boldsymbol{\nabla}\boldsymbol{\Theta}_{k,3}\boldsymbol{\nabla}^{\mathrm{T}})\big)\boldsymbol{\Omega}_2^{\mathrm{T}}\Big]\boldsymbol{\Upsilon}_k. \tag{29}$$

By combining conditions (14)–(16) with (28) and (29), it is the case that

$$\dot{\mathbf{V}}(t) + \boldsymbol{\beta}\mathbf{V}(t) < 0 \tag{30}$$

for any $t \in [t_s, t_{s+1})$ and $\boldsymbol{\Upsilon}_k \neq \mathbf{0}$.

For the switching instant t_s of the topology structure, suppose $\varsigma(t_s) = k$ and $\varsigma(t_s^-) = r$ for any $k \neq r \in \boldsymbol{\aleph}$. Hence, it follows from Lemma 4 the construction of the TDTVLF (19) that

$$\begin{aligned}
\mathbf{V}(t_s) &= \mathbf{V}_k\big(\tilde{\boldsymbol{\xi}}(t_s)\big) \\
&= \tilde{\boldsymbol{\xi}}^{\mathrm{T}}(t_s)(\boldsymbol{\wp}_k \otimes \mathbf{P}_{k,1})\tilde{\boldsymbol{\xi}}(t_s) \\
&\leq \boldsymbol{\mu}\tilde{\boldsymbol{\xi}}^{\mathrm{T}}(t_s)(\boldsymbol{\wp}_k \otimes \mathbf{P}_{r,2})\tilde{\boldsymbol{\xi}}(t_s) \\
&\leq \boldsymbol{\mu}\boldsymbol{\lambda}_{\max}\big((\boldsymbol{\wp}_r \otimes \mathbf{P}_{r,2})^{-1}(\boldsymbol{\wp}_k \otimes \mathbf{P}_{r,2})\big)\tilde{\boldsymbol{\xi}}^{\mathrm{T}}(t_s^-)(\boldsymbol{\wp}_r \otimes \mathbf{P}_{r,2})\tilde{\boldsymbol{\xi}}(t_s^-) \\
&\leq \boldsymbol{\mu}\boldsymbol{\tau}\mathbf{V}(t_s^-).
\end{aligned} \tag{31}$$

Moreover, since $\boldsymbol{\wp}_k > 0$ and $\mathbf{P}_k(t) > 0$, there exist positive scalars $\underline{\boldsymbol{z}}$ and $\overline{\boldsymbol{z}}$ such that

$$\underline{\boldsymbol{z}}\|\tilde{\boldsymbol{\xi}}(t)\|^2 \leq \mathbf{V}(t) \leq \overline{\boldsymbol{z}}\|\tilde{\boldsymbol{\xi}}(t)\|^2. \tag{32}$$

Then, for any $t \in [t_s, t_{s+1})$, integrating inequalities (30)–(32) gives

$$\begin{aligned}
\mathbf{V}(t) &\leq e^{-\boldsymbol{\beta}(t-t_s)}\mathbf{V}(t_s) \\
&\leq \boldsymbol{\mu}\boldsymbol{\tau}e^{-\boldsymbol{\beta}(t-t_s)}\mathbf{V}(t_s^-) \\
&\leq \cdots \\
&\leq (\boldsymbol{\mu}\boldsymbol{\tau})^{\frac{t-t_0}{\boldsymbol{\varsigma}_1}}e^{-\boldsymbol{\beta}(t-t_0)}\mathbf{V}(t_0) \\
&\leq e^{(-\boldsymbol{\beta}+\frac{\ln(\boldsymbol{\mu}\boldsymbol{\tau})}{\boldsymbol{\varsigma}_1})(t-t_0)}\mathbf{V}(t_0).
\end{aligned} \tag{33}$$

By the dwell time constraint (18), it can be inferred that $-\boldsymbol{\beta} + \frac{\ln(\boldsymbol{\mu}\boldsymbol{\tau})}{\boldsymbol{\varsigma}_1} < 0$, and thus the exponential stability is guaranteed for system (9). Meanwhile, the DN (1) can realize the TVF $\boldsymbol{y}(t)$. This completes the proof. □

Remark 7. *The nonsingular transformation matrix $\mathfrak{F}$ plays an important role in the proposed TVF analysis and protocol design. For each directed topology containing a spanning tree, zero is a simple eigenvalue of the Laplacian matrix $\mathcal{L}_\ell$ and $\mathbf{1}_\mathbf{N}$ is the associated right eigenvector. Therefore, a nonsingular matrix $\mathfrak{F} = [\mathbf{1}_\mathbf{N}, \tilde{\mathfrak{F}}]$ can be selected*

to separate the macroscopic formation motion from the reduced formation error dynamics. As pointed out in [16], the selection of $\mathfrak{F}$ is non-unique, and any nonsingular matrix whose first column is $\mathbf{1_N}$ is admissible, for example, $\mathfrak{F} = \begin{bmatrix} 1 & 0_{1\times(\mathbf{N}-1)} \\ \mathbf{1}_{\mathbf{N}-1} & \mathbf{I}_{\mathbf{N}-1} \end{bmatrix}$. Under this transformation, the reduced Laplacian matrix $\bar{\mathcal{L}}_k = \bar{\mathfrak{F}}\mathcal{L}_k\tilde{\mathfrak{F}}$ contains all nonzero eigenvalue information of $\mathcal{L}_k$ and is used to characterize the convergence of the formation error.

Remark 8. *In this research, a TDTVLF framework is constructed for the TVF control of general DNs with switching topologies, where only low-dimensional matrix conditions are required in Theorem 1 to guarantee the desired TVF performance. This feature renders the developed method more applicable to formation control investigations for large-scale directed networks. In addition, by defining $\mathbf{P}_k(t) = \mathbf{P}^{-1}$ with $\mathbf{P} > 0$, it is evident that the proposed TDTVLF (19) encompasses the existing approaches in [16, 27] for the formation control and consensus exploration of multi-agent systems with switching topologies as special cases. By simply setting $\boldsymbol{y}(t) \equiv 0$, the TVF control problem investigated herein degenerates into a consensus control of DNs under switching topologies. Another core contribution of the present study lies in presenting the decoupling property of the Kronecker product in formula (13), which provides a foundation for constructing low-dimensional TVF control criteria for formation control of large-scale DNs.*

Remark 9. *In a network, the coupling strength governs the collective dynamical behavior of the whole network. A larger coupling strength generally corresponds to stronger interactions among nodes, whereas a smaller coupling strength yields more independent node dynamics and preserves higher autonomy for individual agents within the network [25]. With other controller parameters fixed, it can be observed from control protocol (3) that maintaining a larger coupling strength will lead to higher control cost. Accordingly, the selection of coupling strength requires a trade-off between satisfactory formation performance and allowable control cost. As for the dwell time ς_1, its value is chosen to exceed the theoretical threshold derived from the dwell time constraint in condition (18), such that exponential convergence of the switched formation error system can be guaranteed (see formula (33)). Naturally, a larger value of the dwell time ς_1 corresponds to slower topology switching.*

Remark 10. *From an engineering perspective, the proposed control protocol shows promising applicability for multi-robot cooperative systems, unmanned aerial vehicle formations, as well as intelligent transportation systems. For these application scenarios, each node only requires local information including its own formation error and relative formation error measurements from neighboring nodes under the current directed communication topology. The topology-dependent gain together with the dwell-time condition offers a feasible alternative for controller updates when communication links undergo switching caused by node mobility, obstacles, bandwidth constraints, or time-varying network quality.*

4. Simulation Example

This section introduces a illustrative example to demonstrate the validity of the achieved theoretical results.

Example 1. *Consider a swarm of 20 unicycle-type autonomous mobile robots [28, 29], with the kinematics of the i-th robot characterized by:*

$$\begin{cases} \dot{\bar{\mathbf{x}}}_i(t) = \cos\big(\phi_i(t)\big)v_i(t), \\ \dot{\bar{\mathbf{w}}}_i(t) = \sin\big(\phi_i(t)\big)v_i(t), \\ \dot{\phi}_i(t) = \sigma_i(t), \end{cases} \tag{34}$$

where $\bar{\mathbf{x}}_i(t)$ and $\bar{\mathbf{w}}_i(t)$ stand for the Cartesian position coordinates of the i-th robot's center of mass; $\phi_i(t)$ defines the heading angle in the inertial frame; $v_i(t)$ refers to the linear velocity; and $\sigma_i(t)$ is the angular velocity.

Define symbols $\boldsymbol{x}_i(t) = \mathbf{col}\big(\bar{\mathbf{x}}_i(t), v_i^{\mathfrak{x}}(t), \bar{\mathbf{w}}_i(t), v_i^{\mathfrak{y}}(t)\big)$ and $\boldsymbol{u}_i(t) = \mathbf{col}(u_i^{\mathfrak{x}}, u_i^{\mathfrak{y}})$. Specifically, $v_i^{\mathfrak{x}}(t)$ and $v_i^{\mathfrak{y}}(t)$ denote the linear velocity components along the X-axis and Y-axis, while $u_i^{\mathfrak{x}}, u_i^{\mathfrak{y}}$ correspond to the control input components aligned with the two axes correspondingly. Then, with the dynamic feedback linearization scheme presented in reference [29], the linearized multirobot dynamics of (34) can be formulated by the DN (1) with

$$\mathbf{A} = \begin{bmatrix} 0 & 1 & 0 & 0 \\ 0 & 0 & 0 & 0 \\ 0 & 0 & 0 & 1 \\ 0 & 0 & 0 & 0 \end{bmatrix}, \ \mathbf{B} = \begin{bmatrix} 0 & 0 \\ 1 & 0 \\ 0 & 0 \\ 0 & 1 \end{bmatrix}.$$

Clearly, it is verified that $\mathbf{rank}(\mathbf{B}) = 2$, and thus the matrix $\mathbf{B}$ is of full column rank. The interaction topology, which switches between two directed graphs $\mathcal{G}_1$ and $\mathcal{G}_2$, is depicted in Figure 2. It can be verified that both $\mathcal{G}_1$ and $\mathcal{G}_2$ contain a spanning tree. The anticipated TVF vector associated with the i-th node is defined by

$$\boldsymbol{y}_i(t) = \begin{bmatrix} 15\cos 2t + \frac{\pi(i-1)}{10} \\ -30\sin 2t + \frac{\pi(i-1)}{10} \\ 15\sin 2t + \frac{\pi(i-1)}{10} \\ 30\cos 2t + \frac{\pi(i-1)}{10} \end{bmatrix}, \ i \in \mathbb{S}_{[1,20]}.$$

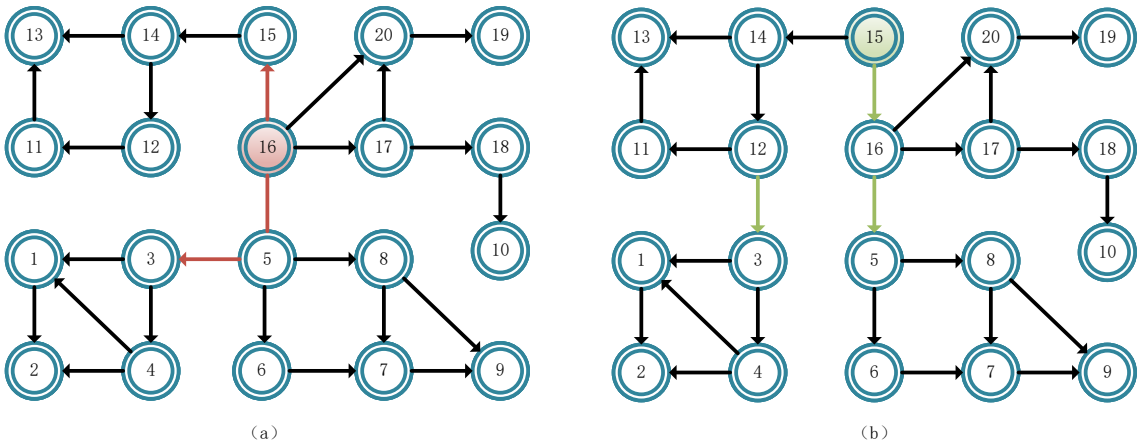


Figure 2. Interaction topologies ((**a**) $\mathcal{G}_1$; (**b**) $\mathcal{G}_2$) for the 20 unicycle-type autonomous mobile robots.

To guarantee the formation constraint (8) in Remark 3, the corresponding formation compensation signal is selected as

$$\boldsymbol{c}_i(t) = \begin{bmatrix} -60\cos 2t + \frac{\pi(i-1)}{10} \\ -60\sin 2t + \frac{\pi(i-1)}{10} \end{bmatrix}, \ i \in \mathbb{S}_{[1,20]}.$$

In what follows, it is illustrated that the presented formation control strategy enables twenty unicycle robots to cooperatively form a circular configuration over the XY plane, where their mass-center coordinates $\mathfrak{x}_i(t)$ and $\mathfrak{y}_i(t)$ act as reference positions. In the implementation, to keep the entire TVF within the observable range, $\mathbf{K}_1$ is selected as

$$\mathbf{K}_1 = \begin{bmatrix} -0.1685 & -1.9375 & 0.9883 & 0.2456 \\ -0.5343 & -0.7715 & 0.1665 & -1.0625 \end{bmatrix}$$

to assign the eigenvalues of $\mathbf{A}_c = \mathbf{A} + \mathbf{B}\mathbf{K}_1$ at -1, -2 and ± 0.5j.

According to the directed graph $\mathcal{G}_1$ and $\mathcal{G}_2$ in Figure 2, it can be calculated that

$$\begin{aligned} \boldsymbol{\varkappa}_{1,1} &= \boldsymbol{\lambda}_{\min}\big((\bar{\mathcal{L}}_1 + \wp_1^{-1}\bar{\mathcal{L}}_1^{\mathrm{T}}\wp_1)\big) = 1.9635, \\ \boldsymbol{\varkappa}_{1,2} &= \boldsymbol{\lambda}_{\max}\big((\wp_1^{-1}\bar{\mathcal{L}}_1^{\mathrm{T}}\wp_1\bar{\mathcal{L}}_1)\big) = 9.0047, \\ \boldsymbol{\varkappa}_{2,1} &= \boldsymbol{\lambda}_{\min}\big((\bar{\mathcal{L}}_2 + \wp_2^{-1}\bar{\mathcal{L}}_2^{\mathrm{T}}\wp_2)\big) = 1.9629, \\ \boldsymbol{\varkappa}_{2,2} &= \boldsymbol{\lambda}_{\max}\big((\wp_2^{-1}\bar{\mathcal{L}}_2^{\mathrm{T}}\wp_2\bar{\mathcal{L}}_2)\big) = 9.0400, \\ \boldsymbol{\tau} &= \max\big\{\boldsymbol{\lambda}_{\max}\big(\wp_r^{-1}\wp_k\big), k \neq r \in \aleph\big\} = 2, \\ &\min\big\{\mathbf{Re}\big(\boldsymbol{\lambda}_i(\bar{\mathcal{L}}_1\big), \ i \in \mathbb{S}_{[1,19]}\big\} = 1, \\ &\min\big\{\mathbf{Re}\big(\boldsymbol{\lambda}_i(\bar{\mathcal{L}}_2\big), \ i \in \mathbb{S}_{[1,19]}\big\} = 1. \end{aligned}$$

Choose the parameters $\boldsymbol{\alpha} = 0.1$, $\boldsymbol{\beta} = 0.8$, $\boldsymbol{\eta}_1 = \boldsymbol{\eta}_2 = 0.1$ and $\varsigma_1 = 1 > \frac{\ln \boldsymbol{\mu}\boldsymbol{\tau}}{\boldsymbol{\beta}} = 0.8664$. By applying Theorem 1, we have

$$\mathbf{K}_{2,1} = \begin{bmatrix} 3.1111 & 3.7688 & -0.4175 & -0.1832 \\ 1.4306 & -0.1870 & 6.0377 & 5.2800 \end{bmatrix},$$

$$\mathbf{K}_{2,2} = \begin{bmatrix} 3.1162 & 3.7661 & -0.4124 & -0.1824 \\ 1.4271 & -0.1873 & 6.0369 & 5.2748 \end{bmatrix},$$

$$\mathbf{Z}_1 = \begin{bmatrix} 329.0563 & -4.9005 \\ -4.9005 & 376.2395 \end{bmatrix},$$

$$\mathbf{Z}_2 = \begin{bmatrix} 328.5412 & -4.5321 \\ -4.5321 & 374.8155 \end{bmatrix},$$

$$\mathbf{Q}_1 = \begin{bmatrix} 0.0174 & 0.0095 & 0.0078 & 0.0039 \\ 0.0095 & 0.0114 & -0.0010 & -0.0003 \\ 0.0078 & -0.0010 & 0.0265 & 0.0160 \\ 0.0039 & -0.0003 & 0.0160 & 0.0140 \end{bmatrix},$$

$$\mathbf{Q}_2 = \begin{bmatrix} 0.0175 & 0.0095 & 0.0078 & 0.0039 \\ 0.0095 & 0.0115 & -0.0010 & -0.0004 \\ 0.0078 & -0.0010 & 0.0265 & 0.0161 \\ 0.0039 & -0.0004 & 0.0161 & 0.0141 \end{bmatrix}.$$

Table 1 tabulates the initial states for the 20 agents. Figure 3 portrays the evolution strategy of switching signal, where subsystem 1 corresponds to the directed graph $\mathcal{G}_1$, while subsystem 2 corresponds to the directed graph $\mathcal{G}_2$. Then, with the formation control protocol (3), Figure 4 demonstrates the evolution strategy of the formation errors associated with 20 nodes. Figure 6 gives three-dimensional time evolution trajectories of state components $\bar{\mathbf{x}}_i(t)$ and $\bar{\mathbf{w}}_i(t)$. Besides, Figure 5 depicts the snapshots of formation with 20 nodes at six representative time instant, i.e., $t = 1s$, $t = 3s$, $t = 7s$, $t = 15s$, $t = 25s$ and $t = 30s$, under the proposed controller. Each subplot records the planar position of every node with its unique index. Together with the formation error curves in Figure 4, these snapshots demonstrate convergence toward the prescribed time-varying formation.

Table 1. Initial states of the 20 agents.

Agent i	$\bar{\mathbf{x}}_i(0)$	$v_i^{\mathfrak{x}}(0)$	$\bar{\mathbf{w}}_i(0)$	$v_i^{\mathfrak{y}}(0)$	**Agent** i	$\bar{\mathbf{x}}_i(0)$	$v_i^{\mathfrak{x}}(0)$	$\bar{\mathbf{w}}_i(0)$	$v_i^{\mathfrak{y}}(0)$
1	1.00	8.60	0.40	7.20	2	1.34	10.00	0.78	9.00
3	1.12	7.40	−0.40	−1.20	4	−0.76	−1.38	1.16	0.60
5	1.70	−1.92	1.50	1.32	6	2.74	−0.66	0.50	1.12
7	−1.44	−3.00	2.40	−1.66	8	1.18	0.54	−0.40	1.20
9	1.60	1.80	−1.04	0.72	10	−1.60	1.80	1.40	7.20
11	1.00	0.60	0.40	0.92	12	1.34	0.70	0.78	0.78
13	1.12	1.40	0.40	1.20	14	0.76	1.38	1.16	0.60
15	1.70	0.52	1.10	1.32	16	2.00	1.66	1.50	1.12
17	1.44	2.60	2.40	1.66	18	1.18	0.54	1.64	1.20
19	1.60	1.80	1.04	1.92	20	1.60	1.80	1.40	1.20

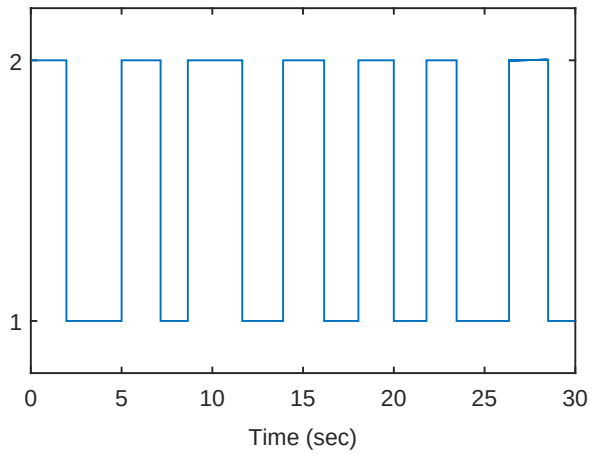


Figure 3. Evolution strategy of switching signal.

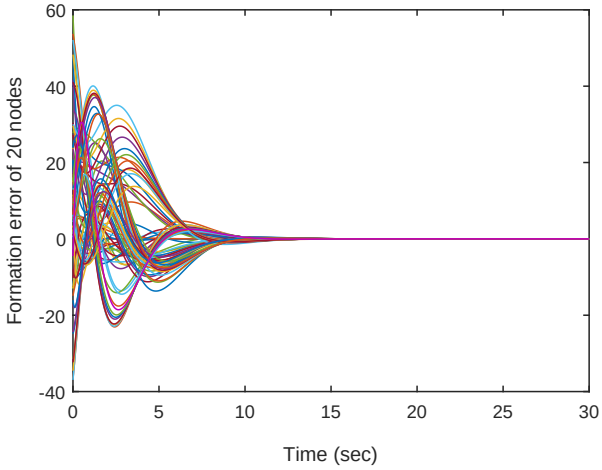


Figure 4. Formation error of 20 nodes.

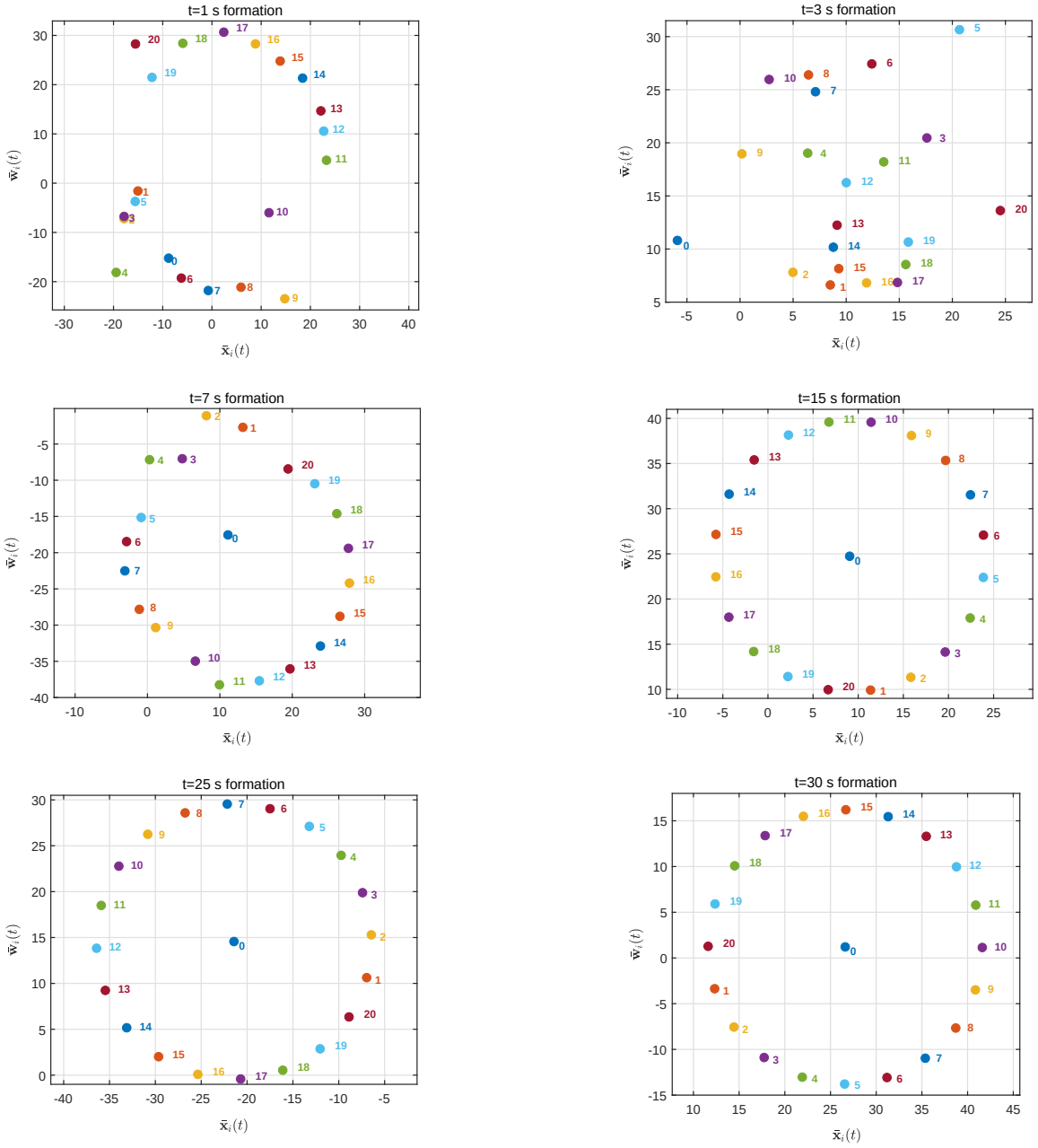


Figure 5. Position snapshots of the 20 agents at different time instants.

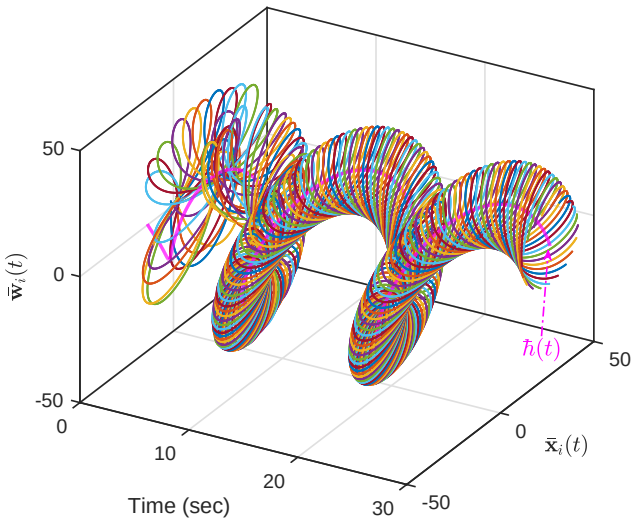


Figure 6. Three-dimensional time evolution trajectories of state components $\bar{\mathbf{x}}_i(t)$ and $\bar{\mathbf{w}}_i(t)$.

5. Conclusions

This work studied the TVF control problem for a category of DNs with switching interaction topologies. For this purpose, a distributed control protocol with a topology-dependent coupling gain was proposed. By introducing a nonsingular coordinate transformation, the formation control problem has been transformed into the stability analysis of a switched system. Then, by constructing a delicate TDTVLF framework, the corresponding formation control criterion is derived to guarantee the exponential convergence of the formation error. The numerical example concerning multi-robot coordinated formation further substantiates the efficacy and applicability of the elaborately constructed control protocol. Although a novel TVF control paradigm based on the TDTVLF framework has been established in this work, the derivation of a more general framework remains to be further explored. Note that practical networks are subject to various unfavorable factors, including limited communication resources, communication delays, actuator saturation, external disturbances, and malicious attacks [30–33]. Motivated by these practical challenges, future work will be devoted to extending the proposed design approach to robust and secure TVF control, developing its event-triggered implementation, as well as conducting experimental validations on physical multi-robot platforms.

Author Contributions

B.Z.: investigation, writing—original draft preparation; H.S.: supervision, writing—reviewing and editing; Y.L.: investigation, methodology; P.W.: investigation, methodology; G.M.D.: conceptualization, methodology. All authors have read and agreed to the published version of the manuscript.

Funding

This work was supported by the National Natural Science Foundation of China under Grants 62203080, the Natural Science Foundation of Liaoning Province under Grant 2026-MS-103, the China Postdoctoral Science Foundation under Grant 2023M740467, and the Open Project Program of Center for Applied Mathematics of Fujian Province, Fuzhou University under Grant S20240903.

Data Availability Statement

Not applicable.

Conflicts of Interest

The authors declare no conflict of interest.

Use of AI and AI-Assisted Technologies

No AI tools were utilized for this paper.

References

1. Yildirim, E.; Yucelen, T. Control of Multiagent Networks with Misbehaving Nodes over Directed Graph Topologies. *IEEE Trans. Control Netw. Syst.* **2025**, *12*, 1521–1530. https://doi.org/10.1109/tcns.2025.3526569.
2. Gu, H.; Liu, P.; Lu, J.; et al. PID Control for Synchronization of Complex Dynamical Networks with Directed Topologies. *IEEE Trans. Cybern.* **2021**, *51*, 1334–1346. https://doi.org/10.1109/tcyb.2019.2902810.
3. Chen, J.; Wang, Y.; Wang, F. Observer-Based Finite-Horizon H_∞ Consensus Control of Multi-Agent Systems under Multi-round-Robin Scheduling. *Intell. Control* **2026**, *2*, 3. https://doi.org/10.53941/ic.2026.100003.
4. Ning, Z.; Xie, L. A Survey on Multi-Agent Reinforcement Learning and Its Application. *J. Autom. Intell.* **2024**, *3*, 73–91. https://doi.org/10.1016/j.jai.2024.02.003.
5. Niu, B.; Zhao, X.; Gao, Y.; et al. Adaptive Fixed-Time Event-Triggered Consensus Tracking Control for Robotic Multiagent Systems. *IEEE Trans. Syst. Man Cybern. Syst.* **2025**, *55*, 7238–7246. https://doi.org/10.1109/tsmc.2025.3582649.
6. Oh, K.K.; Park, M.C.; Ahn, H.S. A Survey of Multi-Agent Formation Control. *Automatica* **2015**, *53*, 424–440. https://doi.org/10.1016/j.automatica.2014.10.022.
7. Balch, T.; Arkin, R.C. Behavior-Based Formation Control for Multirobot Teams. *IEEE Trans. Robot. Autom.* **1998**, *14*, 926–939. https://doi.org/10.1109/70.736776.
8. Lewis, M.A.; Tan, K.H. High Precision Formation Control of Mobile Robots Using Virtual Structures. *Auton. Robot.* **1997**, *4*, 387–403. https://doi.org/10.1023/a:1008814708459.
9. Das, A.K.; Fierro, R.; Kumar, V.; et al. A Vision-Based Formation Control Framework. *IEEE Trans. Robot. Autom.* **2002**, *18*, 813–825. https://doi.org/10.1109/tra.2002.803463.
10. Ren, W.; Beard, R.W. Consensus Seeking in Multiagent Systems under Dynamically Changing Interaction Topologies. *IEEE Trans. Autom. Control.* **2005**, *50*, 655–661. https://doi.org/10.1109/tac.2005.846556.
11. Ren, W. Consensus Strategies for Cooperative Control of Vehicle Formations. *IET Control Theory Appl.* **2007**, *1*, 505–512. https://doi.org/10.1049/iet-cta:20050401.
12. Fax, J.A.; Murray, R.M. Information Flow and Cooperative Control of Vehicle Formations. *IEEE Trans. Autom. Control.* **2004**, *49*, 1465–1476. https://doi.org/10.1109/tac.2004.834433.
13. Wang, K.; Wu, W.; Tong, S. Adaptive Neural Network Event-Triggered Secure Formation Control of Nonholonomic Mobile Robots Subject to Deception Attacks. *J. Autom. Intell.* **2024**, *3*, 260–268. https://doi.org/10.1016/j.jai.2024.10.002.
14. Ma, C.; Zhang, J. On Formability of Linear Continuous-Time Multi-Agent Systems. *J. Syst. Sci. Complex.* **2012**, *25*, 13–29. https://doi.org/10.1007/s11424-012-0108-3.
15. Zhou, S.; Sun, D. Group Formation Tracking for Heterogeneous Linear Multi-Agent Systems under Switching Topologies. *J. Autom. Intell.* **2025**, *4*, 108–114. https://doi.org/10.1016/j.jai.2025.03.003. Erratum in *J. Autom. Intell.* **2026**, *5*, 268–269. https://doi.org/10.1016/j.jai.2026.09.001.
16. Dong, X.; Hu, G. Time-Varying Formation Control for General Linear Multi-Agent Systems with Switching Directed Topologies. *Automatica* **2016**, *73*, 47–55. https://doi.org/10.1016/j.automatica.2016.06.024.
17. Wang, R.; Dong, X.; Li, Q.; et al. Distributed Time-Varying Formation Control for Linear Swarm Systems with Switching Topologies Using an Adaptive Output-Feedback Approach. *IEEE Trans. Syst. Man Cybern. Syst.* **2019**, *49*, 2664–2675. https://doi.org/10.1109/tsmc.2017.2765203.
18. Deng, C.; Che, W.W. Fault-Tolerant Fuzzy Formation Control for a Class of Nonlinear Multiagent Systems under Directed and Switching Topology. *IEEE Trans. Syst. Man Cybern. Syst.* **2021**, *51*, 5456–5465. https://doi.org/10.1109/tsmc.2019.2954870.
19. Wei, L.; Chen, M.; Shi, S. Dynamic Event-Triggered Consensus Cost-Based Switching Control for UAV Formation with Disturbances. *IEEE Trans. Intell. Veh.* **2024**, *9*, 3531–3543. https://doi.org/10.1109/tiv.2023.3344606.
20. Zhao, S.; Yu, J.; Zhao, Z.; et al. Co-Design of Fault Detection and Bipartite Time-Varying Formation Control for a Class of Fuzzy Multiagent Systems under Switching Topology. *IEEE Trans. Syst. Man Cybern. Syst.* **2025**, *55*, 8850–8862. https://doi.org/10.1109/tsmc.2025.3612419.
21. Allerhand, L.I.; Shaked, U. Robust Stability and Stabilization of Linear Switched Systems with Dwell Time. *IEEE Trans. Autom. Control.* **2011**, *56*, 381–386. https://doi.org/10.1109/tac.2010.2097351.
22. Saboori, I.; Khorasani, K. H_∞ Consensus Achievement of Multi-Agent Systems with Directed and Switching Topology Networks. *IEEE Trans. Autom. Control.* **2014**, *59*, 3104–3109. https://doi.org/10.1109/tac.2014.2358071.
23. Boyd, S.; El Ghaoui, L.; Feron, E.; et al. *Linear Matrix Inequalities in System and Control Theory*; Society for Industrial and Applied Mathematics: Philadelphia, PA, USA, 1994. https://doi.org/10.1137/1.9781611970777.
24. Bernstein, D.S. *Matrix Mathematics*; Princeton University Press: Princeton, NJ, USA, 2009. https://doi.org/10.1515/9781400833344.
25. Sang, H.; Wang, P.; Zhao, Y.; et al. Delay-Dependent but ($\mathcal{N}$)-Independent Pinning Synchronization Control for Switched Delayed Directed Networks. *SIAM J. Control Optim.* **2025**, *63*, 699–726. https://doi.org/10.1137/23m1571502.
26. Sang, H.; Cui, C.; Wang, P.; et al. Further on Pinning Quasi-Synchronization of Switched Directed Networks with Event-Triggered Communication. *IEEE Trans. Autom. Control.* **2025**, *70*, 6127–6134. https://doi.org/10.1109/tac.2025.3552027.
27. Wen, G.; Zheng, W.X. On Constructing Multiple Lyapunov Functions for Tracking Control of Multiple Agents with

Switching Topologies. *IEEE Trans. Autom. Control.* **2019**, *64*, 3796–3803. https://doi.org/10.1109/tac.2018.2885079.

28. Ge, X.; Han, Q.L. Distributed Formation Control of Networked Multi-Agent Systems Using a Dynamic Event-Triggered Communication Mechanism. *IEEE Trans. Ind. Electron.* **2017**, *64*, 8118–8127. https://doi.org/10.1109/tie.2017.2701778.
29. Liu, T.; Jiang, Z.P. Distributed Formation Control of Nonholonomic Mobile Robots without Global Position Measurements. *Automatica* **2013**, *49*, 592–600. https://doi.org/10.1016/j.automatica.2012.11.031.
30. Tajudeen, M.M.; Banu, K.A.; Tatar, N.E.; et al. Observer-Based Secure H_∞ Control for Networked Control Systems with Multiple Disturbances, Actuator Failures, and Deception Attacks under Adaptive Event-Triggered Mechanism. *Sci. Rep.* **2026**, *16*, 10092. https://doi.org/10.1038/s41598-026-36662-4.
31. Tajudeen, M.M.; Banu, K.A.; Tatar, N.E.; et al. Observer Based Security Control for Interval Type-2 Fuzzy Networked System Subject to Hybrid Attacks via Resilient Event-Triggered Scheme and Its Application. *J. Frankl. Inst.* **2026**, *363*, 108777. https://doi.org/10.1016/j.jfranklin.2026.108777.
32. Banu, K.A.; Aparna, T.; Tajudeen, M.M.; et al. Secure Event-Triggered Control of Nonlinear Networked Systems via Interval Type-2 Fuzzy Observer Design. *Sci. Rep.* **2026**, *16*, 24221. https://doi.org/10.1038/s41598-026-53335-4.
33. Suresh, M.; Samidurai, R.; Banu, K.A.; et al. Exponential Synchronization of T-S Fuzzy Complex-Valued BAM Neural Networks with Mixed Time-Varying Delays via Event-Triggered Control Engineering and Applications. *Neural Netw.* **2026**, *204*, 109254. https://doi.org/10.1016/j.neunet.2026.109254.